Acadlore Transactions on Applied Mathematics and Statistics
https://www.acadlore.com/journals/ATAMS

Application of Laplace Transform Technique of Variable Order to the Generalized Caputo Fractional Model of Second Grade Nanofluid

Zubair Ahmad[1], Saqib Murtaza[2*], Razi Khan[3]

[1] Dipartimento di Matematica e Fisica, Universit'a degli Studi della Campania "Luigi Vanvitelli", 81100 Caserta, Italy
[2] Department of Mathematics, King Mongkut's University of Technology, 10140 Bangkok, Thailand
[3] Department of Mathematics and CEMAT, Instituto Superior Tecnico, 1049-001 Lisbon, Portugal

[*] Correspondence: Saqib Murtaza (saqib.murtaza@mail.kmutt.ac.th)

Received: 07-22-2024 **Revised:** 09-02-2024 **Accepted:** 09-20-2024

Citation: Z. Ahmad, S. Murtaza, and R. Khan, "Application of Laplace transform technique of variable order to the generalized Caputo fractional model of second grade nanofluid," *Acadlore Trans. Appl M ath. Stat.*, v ol. 2, no. 3, pp. 133–149, 2024. https://doi.org/10.56578/atams020302.

© 2024 by the author(s). Published by Acadlore Publishing Services Limited, Hong Kong. This article is available for free download and can be reused and cited, provided that the original published version is credited, under the CC BY 4.0 license.

Abstract: The incorporation of fractional calculus into nanofluid models has proven effective in capturing the complex dynamics of nanofluid flow and heat transfer, thereby enhancing the precision of predictions in this intricate field. In this study, the dynamics of a viscoelastic second-grade nanofluid model are examined through the application of the Laplace transform technique on a vertical plate. Initially, the model is formulated as coupled partial differential equations to describe the second-grade nanofluid system. The governing equations are then rendered dimensionless using appropriate dimensionless parameters. The non-dimensional model is subsequently generalized by introducing a modified Caputo fractional derivative operator. To model a homogenous nanofluid, nanoparticles of Al_2O_3 in nanometer-sized form are suspended in mineral transformer oil. The Laplace transform is employed to solve the momentum, energy, and mass diffusion equations, providing analytical solutions. Graphical and tabular analyses are conducted to assess the influence of various physical parameters—including the fractional order, nanoparticle volume fraction, and time parameter—on the velocity, thermal, and concentration profiles. The results indicate that increasing the nanoparticle volume fraction, fractional order, and time parameter significantly enhances the rate of heat transfer. Additionally, it is observed that the velocity, temperature, and concentration profiles are notably affected by increasing the volume fraction of nanoparticles. The accuracy and reliability of the obtained solutions are validated through comparisons with existing literature. This work advances the understanding of nanofluid dynamics and presents valuable insights for industrial applications, particularly in enhancing heat transfer performance.

Keywords: Generalized Caputo fractional operator; ρ-Laplace transform technique; Mittag-Leffler function; Wright function; Mineral transformer oil

1 Introduction

The Laplace transform is an integral transform method that is used in many fields to solve differential equations and analyze dynamic systems, such as fluid dynamics. The Laplace transform technique converts a time-dependent function into a complex-variable function, that is denoted by s. In this way, differential equations can be transformed into algebraic equations, allowing complex mathematical problems to be solved more easily. The utilization of the Laplace transform method is extremely advantageous in the field of fluid dynamics as it enables a comprehensive comprehension of temporary occurrences and the production of solutions in the time domain for differential equations that dictate fluid flow and heat transfer processes. One can solve Navier-Stokes equations and energy equations more easily by applying the Laplace transform to these equations. Various flow configurations and boundary conditions can be investigated under this model in order to determine the dynamics of transient phenomena such as variations in velocity and temperature distributions over a specific time period. A combination of the Laplace transform, and fractional calculus can help us better understand fluid dynamics. Fractional calculus deals primarily with derivatives and integrals of non-integer orders. It provides a more general method for representing fractal-like patterns, memory effects, and non-local behaviors. Fractional derivatives better represent non-Newtonian behaviors, anomalous diffusion, and viscoelastic effects of fluid dynamics than integer-order derivatives. It is possible to improve the

accuracy of mathematical models that represent real-world fluid flow processes when fractional derivatives and the Laplace transform method are both considered at the same time. Sub-diffusion, super-diffusion, non-Newtonian flows and other complex phenomena in fluids of fractional order can be investigated with this approach. When dealing with complex fluid systems such as viscoelastic fluids and flows through porous media, fractional Laplace transforms are a powerful tool for finding solutions and evaluating fractional differential equations. To summarize, the combination of fractional calculus and Laplace transforms provides a comprehensive way to explain fluid dynamic processes. By incorporating fractional derivatives and transforming differential equations into algebraic equations, a more comprehensive understanding of complex flow processes, non-local effects and unsteady behaviors in many fluid systems can be obtained [1–5].

The wide range of applications of fractional calculus in science and engineering has made it one of the most important topics in mathematics. Fractional calculus offers new ways of describing the dynamics of non-local complex systems. It has been observed that fractional differential operators with non-locality exhibit a stronger memory effect [6–10]. Therefore, a variety of systems have been considered as candidates for applying these operators in order to comprehend the ramifications of non-locality more fully [11–17]. In a recent study conducted by Jarad and Abdeljawad [18], a modified version of the Laplace transform was introduced to accommodate two distinct categories of generalized fractional operators, namely the Riemann and generalized Caputo fractional operators. For the time being, there is no updated Laplace transform for Caputo-Fabrizio and Atangna-Baleanu in the literature. As a result, we used the modified Laplace transform for the generalized Caputo fractional derivative operator to solve a fluid flow problem in a sports phenomenon. Some useful and fruitful studies that are relevant to non-Newtonian problems can be found in the studies [19–21]. In the present work, the authors analyzed the viscoelastic second grade Al_2O_3 based mineral transformer oil nanofluid on a vertical plate. The fractional mathematical model has been developed through the operator of generalized Caputo derivative and then solved by means of the novel ρ-Laplace transform technique. For validation of the present model and obtained solution, the authors compared their results with the already published work.

2 Theory of ρ-Laplace Transform Technique

This section of the manuscript devoted to the fundamental definitions, theorems, and Lemmas of the ρ-Laplace transform technique, which is organized as follow:

Definition 2.1: Let $\eta : [0, \infty) \to \Re$ be a real-valued function then ρ-Laplace transform of η is defined by [18]:

$$\pounds_\rho\{\eta(\tau)\}(q) = \int_0^\infty \exp\left(-q\frac{t^\rho}{\rho}\right)\eta(\tau)\frac{d\tau}{\tau^{1-\rho}}; \quad \rho > 0 \tag{1}$$

for all values of q, the integral is valid.

Theorem 2.2: Let $\eta : [0, \infty) \to \Re$ be a real-valued function such that its ρ-Laplace transform exists. Then

$$\pounds_\rho\{\eta(\tau)\}(q) = \pounds\left\{\eta(\rho\tau)^{\rho^{-1}}\right\}(q) \tag{2}$$

where, $\pounds\{\eta\}$ is the ordinary Laplace transform η.

Convolution Lemma 2.3: Let η and ζ be two piecewise continuous functions at each interval $[0, \tau]$ and of exponential order, then their ρ^* convolution product of η and ζ is given by [18]:

$$(\eta * \zeta)(\tau) = \int_0^\tau \eta\left(\tau^\rho - t^\rho\right)^{-\rho}\zeta(\tau)\frac{dt}{t^{1-\rho}} \tag{3}$$

Then the commutatively of the ρ^* convolution of two function is

$$(\eta * \zeta)(\tau) = (\zeta * \eta)(\tau) \tag{4}$$

ρ-Laplace transform of some elementary functions.

Lemma 2.4: As given in the study [18]:

$$\pounds_\rho\{1\}(q) = \frac{1}{q}, \quad q > 0 \tag{5}$$

$$\pounds_\rho\left\{\tau^\rho\right\}(q) = \rho^{\frac{p}{\rho}}\frac{\Gamma\left(1+\frac{p}{\rho}\right)}{q^{1+\frac{p}{\rho}}}, \quad p \in \Re, \quad q > 0 \tag{6}$$

$$\pounds_\rho\left\{\exp\left(\lambda\frac{\tau^\rho}{\rho}\right)\right\}(q) = \frac{1}{q-\lambda}, \quad q > \lambda \tag{7}$$

2.1 Mittag-Leffler Function

The Mittag-Leffler function, a broader form of exponential functions, plays a crucial role in fractional order calculus. This paper embarks on analyzing the fractional mathematical model of the Navier-Stokes problem, aiming to derive a solution in terms of the Mittag-Leffler function. Therefore, establishing a link between the ρ-Laplace transform and the Mittag-Leffler function is imperative as an initial phase. In fluid dynamics, the Mittag-Leffler function carries substantial physical significance across various domains. The mathematical depiction of the Mittag-Leffler function for a single variable is illustrated in the study [18].

$$E_{\delta}(z) = \sum_{l=0}^{\infty} \frac{z^l}{\Gamma(l\delta + 1)}, z \in \mathbb{C}, \Re(\delta) > 0 \tag{8}$$

In more general form, it is given as [18]:

$$E_{\delta,\gamma}(z) = \sum_{l=0}^{\infty} \frac{z^l}{\Gamma(l\delta + \gamma)}, z \in \mathbb{C}, \Re(\delta) > 0 \tag{9}$$

From Eqs. (8) and (9), the relation $E_{\delta,1}(z) = E_{\delta}(z)$ is obvious.

Lemma 2.5: Assume $\Re(\delta) > 0$ and $\left|\frac{\lambda}{q^{\delta}}\right| < 1$, then:

$$\pounds_{\rho}\left\{E_{\delta}\left(\lambda\left(\frac{\tau^{\rho}}{\rho}\right)^{\delta}\right)\right\} = \frac{q^{\delta-1}}{q^{q} - \lambda} \tag{10}$$

$$\pounds_{\rho}\left\{\left(\frac{\tau^{\rho}}{\rho}\right)^{\delta-1} E_{\delta,\delta}\left(\lambda\left(\frac{\tau^{\rho}}{\rho}\right)^{\delta}\right)\right\} = \left(q^{\delta} - \lambda\right)^{-1} \tag{11}$$

2.2 Generalized Left and Right Caputo Fractional Operator

The left and right generalized Caputo fractional operators are modified as shown in the study [18].

$$\left({}_{a}^{c}\wp^{\gamma,\rho}\eta\right)(\tau) = \frac{1}{\Gamma(n-\gamma)} \int_{z}^{\tau} \left(\frac{\tau^{\rho} - v^{\rho}}{\rho}\right)^{n-\gamma-1} \beta^{n}\eta(v)\frac{dv}{v^{1-\rho}} \tag{12}$$

$$\left({}^{c}\wp_{b}^{\gamma,\rho}\eta\right)(\tau) = \frac{1}{\Gamma(n-\gamma)} \int_{\tau}^{b} \left(\frac{v^{\rho} - \tau^{\rho}}{\rho}\right)^{n-\gamma-1} \left(-\beta^{n}\right)\eta(v)\frac{dv}{v^{1-\rho}} \tag{13}$$

It is worth mentioning that the derivative defined in Eqs. (12) and (13) become Caputo fractional derivative when $\rho = 1$, but for $\rho \to 0$ the derivatives in (12) and (13) approaches to Caputo-Hadamard fractional derivative respectively.

2.3 ρ-Laplace Transform of the Generalized Caputo Fractional Operator

The ρ-Laplace transform of generalized Caputo fractional derivative is given in the following form [22]:

$$\pounds_{\rho}\left\{\left(\wp_{C}^{\gamma,\rho}\eta\right)(\tau)\right\}(q) = q^{\gamma}\left[\pounds_{\rho}\{\eta(\tau)\} - \sum_{j=0}^{n-1} q^{-j-1}\left(\chi^{j}\eta\right)(0)\right] \tag{14}$$

3 Physical Description of the Phenomena

The current research delves into the time-dependent, magnetohydrodynamic (MHD)-free convection flow of a viscoelastic second-grade nanofluid along a vertical plate. The plate is described as an exponentially accelerated isothermal infinite vertical surface, wherein both temperature and mass diffusion undergo variations due to heat absorption. The fluid's conductivity has been scrutinized at a microscopic level, yielding a magnetic Reynolds number below one and a transverse magnetic field surpassing the induced magnetic field. The influence of viscous dissipation and joule heating on the energy equation is deemed negligible. The geometrical representation of the proposed study along with the assumptions is given in Figure 1.

The mathematical model that corresponds to the considered phenomena under consideration is provided in the study [23].

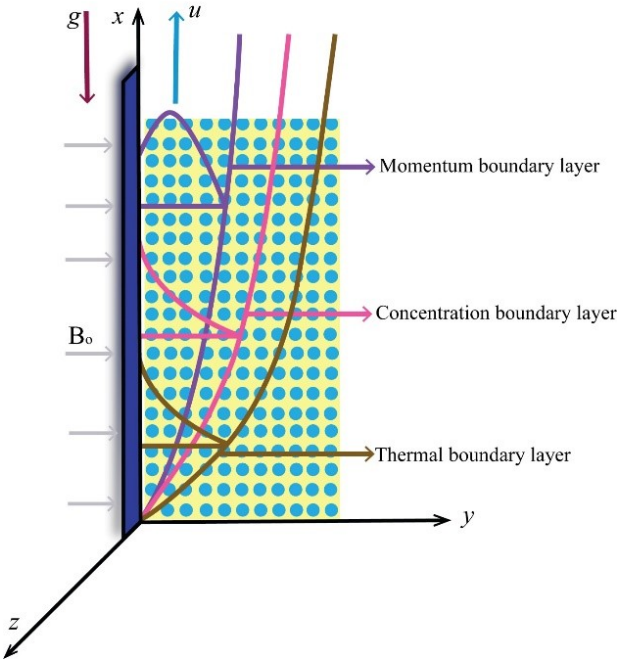

Figure 1. Geometrical description of the flow

$$\rho_{nf}\frac{\partial u(y,t)}{\partial t}=\mu_{nf}\frac{\partial^2 u(y,t)}{\partial y^2}+\alpha_1\frac{\partial^3 u(y,t)}{\partial t\partial y^2}-\sigma_{nf}B_0^2u(y,t)+g\left(\rho\beta_T\right)_{nf}\left(T(y,t)-T_\infty\right)+ g\left(\rho\beta_C\right)_{nf}\left(C(y,t)-C_\infty\right) \tag{15}$$

$$\left(\rho C_p\right)_{nf}\frac{\partial T(y,t)}{\partial t}=k_{nf}\frac{\partial^2 T(y,t)}{\partial y^2} \tag{16}$$

$$\frac{\partial C(y,t)}{\partial t}=D_{nf}\frac{\partial^2 C(y,t)}{\partial y^2} \tag{17}$$

Subjected to the following physical conditions.

$$\left.\begin{array}{ll} u(y,0)=0, & T(y,0)=T_\infty,\\ u(0,t)=U_0H(t)\exp\left(a\frac{t^\rho}{\rho}\right), & T(0,t)=T_w+\left(T_w-T_\infty\right)At^\rho,\\ u(\infty,t)=0, & T(\infty,t)=T_\infty,\\ & C(y,0)=C_\infty,\\ & C(0,t)=C_w+\left(C_w-C_\infty\right)At^\rho,\\ & C(\infty,t)=C_\infty. \end{array}\right\} \tag{18}$$

The correlations between regular fluid, nanofluid and suspended nanoparticles are mathematically stated as [24–27].

Dynamic viscosity:

$$\mu_{nf}=\frac{\mu_f}{(1-\phi)^{2.5}} \tag{19}$$

Density:

$$\rho_{nf}=(1-\phi)\rho_f+\phi\rho_s \tag{20}$$

Mass volumetric expansion:

$$\left(\rho C_p\right)_{vf}=\left(1-\phi\right)\left(\rho C_p\right)_f+\phi\left(\rho C_p\right)_s \tag{21}$$

Thermal volumetric expansion:

$$(\rho\beta_T)_{nf} = (1-\phi)(\rho\beta_T)_f + \phi(\rho\beta_T)_s \tag{22}$$

Electrical conductivity:

$$\sigma_{nf} = \sigma_f \left[1 + \frac{3\left(\frac{\sigma_s}{\sigma_f} - 1\right)\phi}{\left(\frac{\sigma_s}{\sigma_f} + 2\right) - \left(\frac{\sigma_s}{\sigma_f} - 1\right)\phi}\right] \tag{23}$$

Thermal conductivity:

$$k_{nf} = k_f \left[\frac{k_s + 2k_f - 2\phi(k_f - k_s)}{k_s + 2k_f + 2\phi(k_f - k_s)}\right] \tag{24}$$

The experimental values of the thermos-mechanical characteristics of the base fluid mineral transformer oil and suspended nanoparticle aluminum dioxide are given in Table 1.

Table 1. Thermo-mechanical characteristics of regular fluid and nanoparticles [28–30]

	$\boldsymbol{\rho}\,(\mathbf{kg/m^3})$	$\boldsymbol{C_p}\mathbf{(J/kgK)}$	$\boldsymbol{K}\mathbf{(W/mK)}$	$\boldsymbol{\beta_T \times 10^{-5}}\,(\mathbf{K^{-1}})$	$\boldsymbol{\sigma}\mathbf{(\Omega m)^{-1}}$
Mineral Transformer Oil	861	1860	0.157	0.75	1.57×10^{-8}
Al_2O_3	3970	1860	40	0.86	10^{-10}

3.1 Generalization of the Local Model

This portion of the current study will provide a detailed explanation of the process involved in transforming the localized mathematical model into a non-local (generalized) model. The first step involves making the dimensional mathematical model dimensionless by using similarity values. Subsequently, the model is transformed into a time-fractional model by the inclusion of the non-local time derivative, namely the generalized Caputo derivative, in place of the local time derivative [18]. It is essential to note that the non-local model is more advantageous and comprehensive in comparison to the local model for elucidating the memory impact and flow behavior.

Following are the similarity variables for making the system of equations unit less:

$$u^* = \frac{u}{U_0}, \quad \xi = \frac{U_0}{v}y, \quad \tau = \frac{U_0^2}{v}t, \quad \Theta = \frac{T - T_S}{T_p - T_s}, \quad \Phi = \frac{C - C_s}{C_p - C_s} \tag{25}$$

Inserting the above-addressed similarity quantities together with nanofluid expressions; Eqs. (15)–(18) will adopt the shape.

$$\frac{\partial u(\xi,\tau)}{\partial \tau} = b_4 \frac{\partial^2 u(\xi,\tau)}{\partial \xi^2} + \alpha_1^* \frac{\partial^3 u(\xi,\tau)}{\partial t \partial \xi^2} - d_0 u(\xi,\tau) + d_1 \Theta(\xi,\tau) + d_2 \Phi(\xi,\tau) \tag{26}$$

$$\frac{\partial \Theta(\xi,\tau)}{\partial \tau} = \lambda_4 \frac{\partial^2 \Theta(\xi,\tau)}{\partial \xi^2} \tag{27}$$

$$\frac{\partial \Phi(\xi,\tau)}{\partial \tau} = \lambda_5 \frac{\partial^2 \Phi(\xi,\tau)}{\partial \xi^2} \tag{28}$$

with

$$\left.\begin{aligned} &u(\xi,0) = 0, \Theta(\xi,0) = 0, \Phi(\xi,0) = 0, \\ &u(0,\tau) = H(\tau)e^{a\frac{\tau^\rho}{\rho}}, \Theta(0,t) = \tau^\rho, \Phi(0,\tau) = \tau^\rho, \\ &u(\infty,\tau) = 0, \Theta(\infty,\tau) = 0, \Phi(\infty,\tau) = 0. \end{aligned}\right\} \tag{29}$$

The constants and unitless parameters that are produce during calculi are

$$\alpha_1^* = \frac{\alpha_1 U_0^2}{\rho_f v_f b_0}, \quad Gr = \frac{g\left(\beta_T\right)_f v_f \left(T_p - T_s\right)}{U_0^3}, \quad Gm = \frac{g\left(\beta_C\right)_f v_f \left(C_p - C_s\right)}{U_0^3}, \quad M = \frac{\sigma_f B_0^2 v_f}{\rho_f U_0^3},$$

$$\Pr = \frac{\mu_f \left(C_p\right)_f}{k_f}, \quad Sc = \frac{v_f}{D_f}, \quad b_0 = (1-\phi) + \phi\frac{\rho_s}{\rho_f}, \quad b_1 = \mu_f(1-\phi)^{-2.5}, \quad b_2 = (1-\phi) + \phi\frac{(\rho\beta_T)_s}{(\rho\beta_T)_f},$$

$$b_3 = (1-\phi) + \phi\frac{(\rho\beta_c)_s}{(\rho\beta_C)_f}, \quad b_4 = 1 + \frac{3\left(\frac{\sigma_s}{\sigma_f} - 1\right)\phi}{\left(\frac{\sigma_s}{\sigma_f} + 2\right) - \left(\frac{\sigma_s}{\sigma_f} - 1\right)\phi}, \quad b_5 = \frac{b_1}{b_0}, \quad b_6 = \frac{b_4}{b_0}, \quad b_7 = \frac{b_2}{b_0}, \quad b_8 = \frac{b_3}{b_0},$$

$$d_0 = Mb_5, \quad d_1 = b_7 Gr. \quad d_2 = b_8 Gm, \quad \lambda_1 = (1-\phi) + \phi\frac{(\rho C_p)_s}{(\rho C_p)_f}, \quad \lambda_2 = \frac{k_s + 2k_f - 2\phi\left(k_f - k_s\right)}{k_s + 2k_f + 2\phi\left(k_f - k_s\right)},$$

$$\lambda_3 = \frac{\lambda_2}{\lambda_1}, \quad \lambda_4 = \frac{\lambda_3}{\Pr}, \quad \lambda_5 = \frac{(1-\phi)}{Sc}.$$

where, $\alpha_1^*, Gr, Gm, M, \Pr$ and Sc are second grade parameter, thermal Grashof number, mass Grashof number, Magnetic (resistive) parameter, Prandtl number and Schmidth number respectively, while b_0, b_1, b_2, b_3, b_4, b_5, b_6, b_7, b_8, d_0, d_1, d_2, λ_1, λ_2, λ_3, λ_4 and λ_5 are constants. The non-local generalized Caputo model of the unitless governing Eqs. (26)–(28) is given as:

$${}^{c}\wp_{\tau}^{\tau,\rho} u(\xi,\tau) = b_4\frac{\partial^2 u(\xi,\tau)}{\partial\xi^2} + \alpha_1^{*c}\wp_{\tau}^{\tau,\rho}\left(\frac{\partial^2 u(\xi,\tau)}{\partial\xi^2}\right) - d_0 u(\xi,\tau) + d_1\Theta(\xi,\tau) + d_2\Phi(\xi,\tau) \tag{30}$$

$${}^{c}\wp_{\tau}^{\gamma,\rho}\Theta(\xi,\tau) = \lambda_4\frac{\partial^2\Theta(\xi,\tau)}{\partial\xi^2} \tag{31}$$

$${}^{c}\wp_{\tau}^{\gamma,\rho}\Phi(\xi,\tau) = \lambda_5\frac{\partial^2\Phi(\xi,\tau)}{\partial\xi^2} \tag{32}$$

Here the operator of generalized Caputo fractional derivative is defined as

$${}^{c}\wp_{\tau}^{\gamma,\rho}\eta(\zeta,\tau) = \frac{1}{\Gamma(n-\gamma)}\int_a^{\tau}\left(\frac{\tau^{\rho} - t^{\rho}}{\rho}\right)^{n-\gamma-1}\delta^n\eta(u)\frac{du}{u^{1-\rho}} \tag{33}$$

3.1.1 Solution of the concentration equation

Through the application of the ρ-Laplace transform method to the generalized energy equation outlined in Eq. (32); we derive the resulting expression.

$$q^{\gamma}\bar{\Phi}(\xi,q) - \sum_{k=0}^{n-1} q^{\lambda-k-1}\left(\chi^k\Phi\right)(0) - \lambda_5\frac{d^2\bar{\Phi}(\xi,q)}{d\xi^2} = 0 \tag{34}$$

with

$$\left.\bar{\Phi}(0,q) = \rho^{\frac{p}{\rho}}\frac{\Gamma\left(1+\frac{p}{\rho}\right)}{\rho^{1+\frac{p}{\rho}}}, \quad \bar{\Phi}(\infty,q) = 0\right\} \tag{35}$$

Upon solving the summation within the differential Eq. (34) and subsequently applying both the initial and transformed boundary conditions, Eq. (34) can be formulated within the domain of the ρ-Laplace transform.

$$\bar{\Phi}(\xi,q) = \rho^{\frac{p}{\rho}}\frac{\Gamma\left(1+\frac{p}{\rho}\right)}{\rho^{1+\frac{p}{\rho}}}\exp\left(-\xi\sqrt{\lambda_5^{-1}}\sqrt{q^{\gamma}}\right) \tag{36}$$

Applying the inversion technique of ρ-Laplace technique on Eq. (36) by keeping in view the convolution theorem, we reached at $\Phi(\xi,\tau) = \int_0^{\tau}(t-\tau)^{\rho} f(\tau)d\tau$.

Here Ψ is a Wright's function and $f(\tau) = \frac{1}{t}\Psi\left(0, -\frac{\gamma}{2}, -\xi\sqrt{\lambda_5^{-1}}\tau - \frac{\gamma}{2}\right)$.

3.1.2 Solution of the energy equation

Through the application of the ρ-Laplace transform method to the generalized energy equation presented in Eq. (31); we derive the resulting expression.

$$q^{\gamma}\bar{\Theta}(\xi,q)-\sum_{k=0}^{n-1}q^{\lambda-k-1}\left(\chi^{k}\Theta\right)(0)-\lambda_{4}\frac{d^{2}\bar{\Theta}(\xi,q)}{d\xi^{2}}=0 \tag{37}$$

with

$$\left.\bar{\Theta}(0,q)=\rho^{\frac{p}{\rho}}\frac{\Gamma\left(1+\frac{p}{\rho}\right)}{\rho^{1+\frac{p}{\rho}}},\quad \bar{\Theta}(\infty,q)=0\right\} \tag{38}$$

Applying the inversion technique of ρ-Laplace technique on Eq. (37) by keeping in view the convolution theorem, we reached at $\Theta(\xi,\tau)=\int_{0}^{\tau}(t-\tau)^{\rho}g(\tau)d\tau$.

Here Ψ is a Wright's function and $g(\tau)=\frac{1}{t}\Psi\left(0,-\frac{\gamma}{2},-\xi\sqrt{\lambda_{5}^{-1}}\tau-\frac{\gamma}{2}\right)$.

Upon solving the summation within the differential Eq. (37) and subsequently applying both the initial and transformed boundary conditions, Eq. (37) can be expressed within the domain of the ρ-Laplace transform.

$$\bar{\Theta}(\xi,q)=\rho^{\frac{p}{\rho}}\frac{\Gamma\left(1+\frac{p}{\rho}\right)}{q^{1+\frac{p}{\rho}}}\exp\left(-\xi\sqrt{\lambda_{4}}\sqrt{q^{\gamma}}\right) \tag{39}$$

3.1.3 Solution of the momentum equation

Using ρ-Laplace transform to unit less non-local momentum Eq. (30), we reached to

$$\begin{aligned}&q^{\gamma}\bar{u}(\xi,q)-\sum_{k=0}^{n-1}q^{\lambda-k-1}\left(\chi^{k}u\right)(0)-b_{4}\frac{d^{2}\bar{u}(\xi,q)}{d\xi^{2}}+\alpha_{1}^{*}\left(q^{\gamma}-\sum_{k=0}^{n-1}q^{\lambda-k-1}\left(\chi^{k}\right)(0)\right)\frac{d^{2}\bar{u}(\xi,q)}{d\xi^{2}}\\&+d_{0}\bar{u}(\xi,q)-d_{1}\bar{\Theta}(\xi,q)-d_{2}\bar{\Phi}(\xi,q)=0\end{aligned} \tag{40}$$

with

$$\left.\bar{u}(0,q)=\frac{1}{q-\lambda},\quad \bar{u}(\infty,q)=0\right\} \tag{41}$$

Upon solving the summation within the differential Eq. (40) and subsequently applying both the initial and transformed boundary conditions, Eq. (40) can be expressed within the domain of the ρ-Laplace transform.

$$\begin{aligned}\bar{u}(\xi,q)=&\left[\begin{array}{c}\frac{1}{q-\lambda}+\frac{d_{1}\rho^{\frac{p}{\rho}}\Gamma\left(1+\frac{p}{\rho}\right)}{q^{1+\frac{p}{\rho}}\left[\left(\lambda_{4}q^{\gamma}\right)\left(b_{4}+\alpha_{1}^{*}q^{\gamma}\right)-\left(q^{\gamma}+d_{0}\right)\right)}\\+\frac{d_{2}\rho^{\frac{p}{\rho}}\Gamma\left(1+\frac{p}{\rho}\right)}{q^{1+\frac{p}{\rho}}\left[\left(\lambda_{5}^{-1}q^{\gamma}\right)\left(b_{4}+\alpha_{1}^{*}q^{\gamma}\right)-\left(q^{\gamma}+d_{0}\right)\right]}\end{array}\right]\exp\left(-\xi\sqrt{\frac{q^{\gamma}+d_{0}}{b_{4}+\alpha_{1}^{*}q^{\gamma}}}\right)\\&-\frac{d_{1}\rho^{\frac{p}{\rho}}\Gamma\left(1+\frac{p}{\rho}\right)}{q^{1+\frac{p}{\rho}}\left[\left(\lambda_{4}q^{\gamma}\right)\left(b_{4}+\alpha_{1}^{*}q^{\gamma}\right)-\left(q^{\gamma}+d_{0}\right)\right]}\exp\left(-\xi\sqrt{\lambda_{4}}\sqrt{q^{\gamma}}\right)\\&-\frac{d_{2}\rho^{\frac{p}{\rho}}\Gamma\left(1+\frac{p}{\rho}\right)}{q^{1+\frac{p}{\rho}}\left[\left(\lambda_{5}^{-1}q^{\gamma}\right)\left(b_{4}+\alpha_{1}^{*}q^{\gamma}\right)-\left(q^{\gamma}+d_{0}\right)\right]}\exp\left(-\xi\sqrt{\lambda_{5}^{-1}}\sqrt{q^{\gamma}}\right)\end{aligned} \tag{42}$$

Since Eq. (42) in ρ-Laplace transformed domain and in very complex form so it is very difficult to find its inverse ρ-Laplace transform analytically therefore, to obtain the solution of the velocity equation in the time domain, numerical inverse ρ-Laplace transform will be used.

3.2 Nusselt Number

The Nusselt number is a dimensionless parameter used in fluid dynamics to quantify the ratio of convective heat transfer to conductive heat transfer. It plays a crucial role in characterizing the heat transfer behavior between a fluid and a solid surface. The Nusselt number is defined differently for various flow regimes and boundary conditions, but generally, it represents the enhancement or suppression of heat transfer due to convective effects compared to

pure conduction. The relative significance of convective heat transmission over conductive heat transfer can be quantified using the Nusselt number. Convective heat transfer mechanisms in different systems can be evaluated for effectiveness by engineers by comparing Nusselt numbers under various flow conditions. Designing and improving cooling systems, heat exchangers, and other thermal devices requires an understanding of the Nusselt number. Nusselt number correlations are used by engineers to forecast the rates of heat transfer. The dimensionless Nusselt numbers can be expressed mathematically as follows:

$$Nu = \lambda_2 \frac{\partial \Theta}{\partial \xi}\bigg|_{\xi=0} \tag{43}$$

Table 2 presents the computed rate of heat transfer (Nusselt number, Nu) with respect to fractional order, time, and volume fraction parameters. The table indicates both increasing and decreasing trends for different parameters. The Nusselt number decreases with increasing fractional order and time, while it increases as the volume fraction increases. The fractional order is associated with the memory effect and non-local behavior in the system. As the fractional order increases, the system exhibits stronger memory, meaning the current state depends more on its past behavior. This tends to slow down the transfer of heat, reducing the Nusselt number. Similarly, for the time parameter, heat transfer often decreases over time in transient systems as they approach thermal equilibrium. The volume fraction represents the concentration of nanoparticles in the fluid. When the volume fraction increases, more nanoparticles are suspended in the base fluid, which enhances its thermal conductivity. This leads to an increased rate of heat transfer, reflected in a higher Nusselt number. This trend is particularly important in applications where improving heat dissipation is crucial, such as in cooling systems and energy storage. These behaviors highlight the balance between thermal enhancement (via nanoparticles) and the complexity introduced by non-local effects in fractional systems.

Table 2. Nusselt number variation against rooted parameters

γ	τ	ϕ	Nu
0.4	1	0.02	**9.92286**
0.6	1	0.02	**9.90569**
0.4	**1.5**	0.02	**9.89259**
0.4	1	**0.4**	**10.7407**

4 Graphical Analysis

This section of the article focuses on analyzing the physical attributes of the fundamental parameters related to dimensionless momentum, heat, and the diffusion equation. The non-dimensional governing equations have been solved using the ρ-Laplace transform technique.

In Figure 2, the impact of fractional order γ on the mass diffusion profile of the fluid is demonstrated. In the context of concentration fields, the use of a fractional order derivative offers an improved capacity for understanding intricate phenomena, such as anomalous diffusion or non-local interactions. Traditional integer order derivatives describe instantaneous rates of change, but fractional order derivatives account for memory effects and long-range interactions. Consider a hypothetical scenario involving a diffusion phenomenon wherein particles exhibit non-standard movement patterns. In order to achieve a more precise representation of this behavior, the utilization of fractional calculus proves to be beneficial. The utilization of fractional order models allows for the representation of sub-diffusive or super-diffusive phenomena that cannot be adequately explained by integer order models. Classical models make suppositions of those diffusion processes where the rate of diffusion is fixed/constant. In contrast to this, the fractional order model discusses both the standard diffusion (rate of diffusion is fixed) and anomalous diffusion (rate of diffusion is not constant). When the $\gamma < 1$, then the spread rate of the particle is slower than expected and it indicates sub-diffusivity, conversely, when $\gamma > 1$, then the spread rate of the particle is faster than the theoretically expected and it represents super-diffusivity. Fractional order calculus offers a refined approach to characterizing temporal variations in concentrations, particularly in scenarios where the conventional principles of classical calculus may be inadequate. The presence of a more versatile instrument allows for enhanced accommodation to the complexities inherent in specific procedures. Moreover, in the classical derivative, only one mass diffusion profile can be drawn for the fluid under consideration, while in the fractional-order derivative, several mass diffusion profiles can be drawn for the fluid under consideration. Consequently, the non-integer order derivative can provide a variety of fluid layers for fluid analysis. To effectively evaluate their findings, experimentalists should equate their findings to the appropriate layer. The impact of nanoparticles on mass diffusion is determined by the volume fraction ϕ, which affects various factors like surface area, concentration gradients, diffusion channel lengths, and interactions between nanoparticles and the surrounding medium, as displayed in Figure 3. As the concentration

of nanoparticles increases, the surface area available for interactions with other substances proportionally increases. The increased surface area has the potential to boost the adsorption and desorption processes, hence influencing the mass diffusion of different species. It is important to consider that, based on these considerations, one can readily deduce that a rise in the volume fraction of nanoparticles results in an increase in the surface area available for contact. This, in turn, leads to an enhancement in the profile of mass diffusion. In Figure 4, the influence of ρ on the concentration field was assessed, with all other parameters held constant. Based on the data presented in the figure, it can be inferred that the concentration field exhibits an increasing trend as the order ρ increases. As the value of the order parameter ρ increases, there is an observed increase in the concentration field.

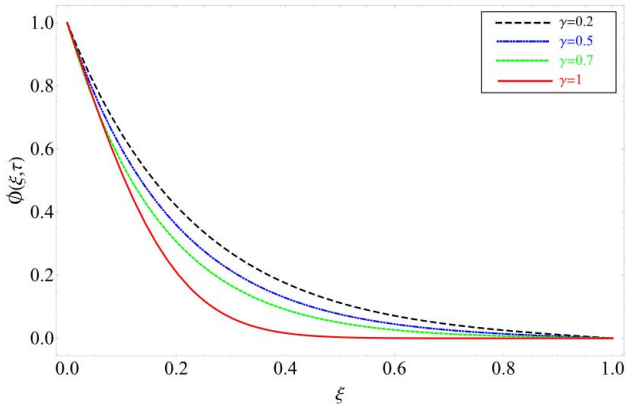

Figure 2. Variation in concentration profile against fractional order γ

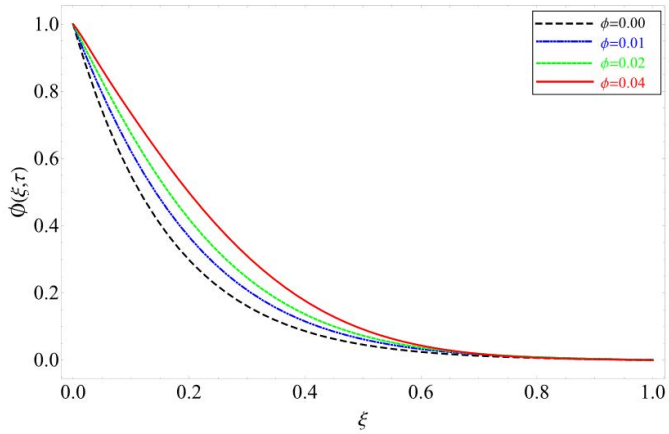

Figure 3. Variation in concentration profile against volume fraction ϕ

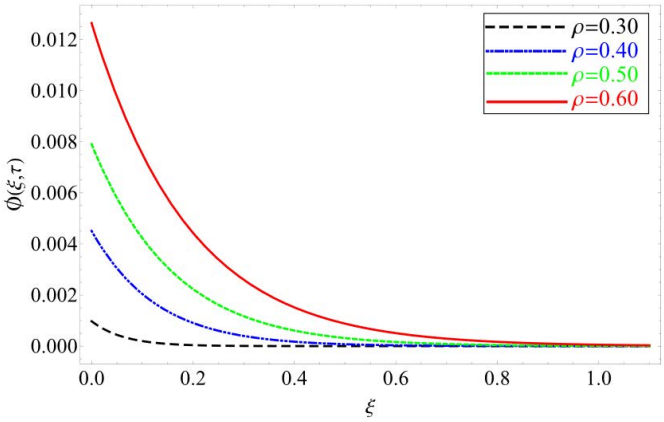

Figure 4. Variation in concentration profile against variable order ρ of Laplace transform

In Figure 5, the impact of fractional order γ on the heat distribution in the fluid is demonstrated. Heat conduction equations traditionally involve integer-order derivatives (e.g., first-order or second-order derivatives). Heat transfer phenomena can be described more nuancedly using fractional order derivatives. These methods have the potential to capture non-local, memory-dependent effects in materials, which may be crucial in certain circumstances. For example, in materials with anomalous heat conduction behavior, where the rate of heat transfer depends on the entire history of temperature changes, fractional order calculus might be more suitable. This is due to the fact that fractional derivatives provide a more thorough description of the behavior of the system by taking into account both the system's current state and its previous states. Fractional order calculus can be useful in temperature profile models of materials or systems where non-local or memory-dependent effects are important for heat transport. It allows for a more accurate representation of complex thermal behaviors. Moreover, in the classical derivative, only one thermal profile can be drawn for the fluid under consideration, while in the fractional-order derivative, several thermal profiles can be drawn for the fluid under consideration. Consequently, the non-integer order derivative can provide a variety of fluid layers for fluid analysis.

Figure 6 illustrates the examination of the temperature profile concerning the magnitude of the volume fraction of Al_2O_3. The volume fraction of nanoparticles in a fluid holds significant importance for heat transfer, with several intriguing phenomena observed as the volume fraction of nanoparticles increases. Notably, the nanofluid's thermal conductivity tends to rise, attributed to the small size of nanoparticles, which enhances the fluid's overall thermal conductivity. This implies that the fluid will transfer heat more effectively. Therefore, an increasing trend is seen in the temperature profile for the volume fraction of nanoparticles. The temperature profile demonstrates a heightened level of heat transfer efficiency in comparison to conventional mineral transformer oil. This enhancement demonstrates significant efficacy in energy conservation and facilitating cooling across multiple sectors. Figure 7 examines the influence of ρ on the temperature distribution, keeping the other parameters constant. The identical pattern has been observed, as depicted in Figure 4. The findings demonstrate that the temperature distribution also exhibits an increase with higher values of the variable ρ.

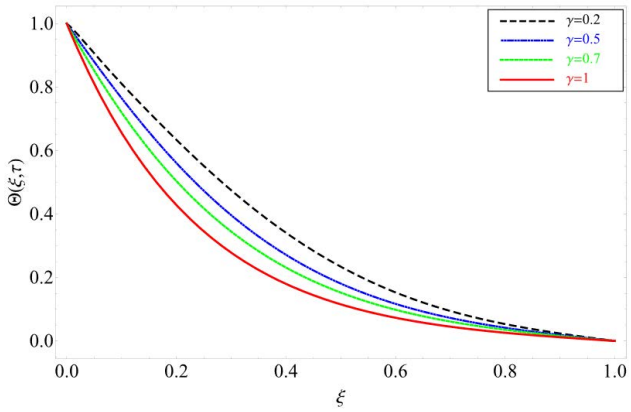

Figure 5. Variation in temperature profile against fractional parameter γ

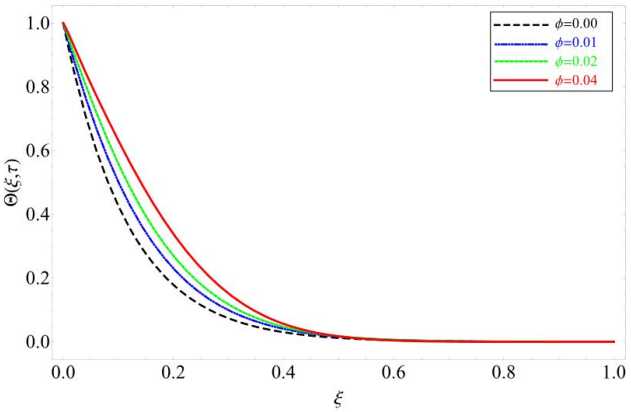

Figure 6. Variation in temperature profile against volume fraction ϕ of nanoparticle

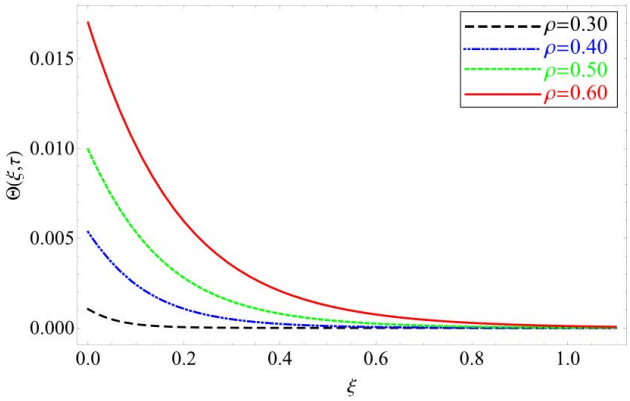

Figure 7. Variation in temperature profile against variable order ρ of Laplace transform

To assess the influence of fractional order on the velocity profile, Figure 8 has been plotted. The velocity profile exhibits a similar trend as depicted in Figure 2 and Figure 5. Traditional models, like Newtonian and non-Newtonian fluids, utilized differential equations of integer order to feature the characteristics of viscosity and elasticity of the fluids. These models assumed a fixed correlation between stress and rate of strain. While fractional calculus enables us to adjust the order of γ of the differential equations to examine the complex behavior of viscosity and elasticity more precisely, a fractional order allows for the modeling of memory and hereditary effects, capturing how past states influence current behavior. Fractional order calculus helps significantly when describing the behavior of time-dependent viscosity of the fluid, one can easily adjust the fractional order parameter to analyze deeply the behavior of viscosity. To examine the effect of the second-grade fluid parameter α_1^* on the velocity profile, Figure 9 has been plotted. As the value of the second-grade fluid parameter increases, the flow characteristics exhibit a greater level of complexity compared to the linear relationship typically observed in Newtonian fluids. When considering transformer oil, which is frequently characterized as a non-Newtonian fluid, an augmentation in the second-order coefficient results in an elevated resistance to shear. The increased resistance to shear exhibited by the oil implies a reduced propensity to undergo deformation or flow when subjected to external forces. Consequently, the velocity profile exhibits a rising pattern due to heightened resistance experienced by the fluid in proximity to the walls or boundaries, resulting in an accumulation of velocity towards the center of the flow. Hence, an upward trend can be observed in the velocity profile. Figure 10 and Figure 11 are plotted to illustrate variations in the velocity profile with respect to thermal and mass Grashof number Gr and Gm respectively. In both figures, the velocity profiles demonstrate increasing variability as the magnitude of Gr and Gm rises. The thermal and mass Grashof numbers Gr and Gm are dimensionless parameters that describe the ratio of buoyancy forces to viscous forces in a fluid flow driven by temperature and concentration differences. As the value of Gr and Gm increases, it signifies a stronger dominance of buoyancy forces relative to viscous forces in the flow. This dominancy of buoyancy forces leads to convective motion, causing fluid particles to move and rearrange more vigorously. Consequently, the velocity profile of the fluid becomes more non-uniform, with higher fluid velocities. Now it depends on the situation and requirement of the researcher or engineer as to what they need, higher viscosity or lower. By using these two parameters, they can easily control the viscosity of the fluid and achieve their desired result.

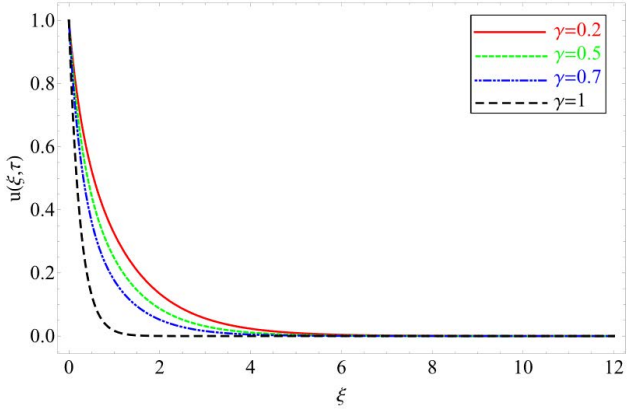

Figure 8. Variation in velocity profile against fractional parameter γ

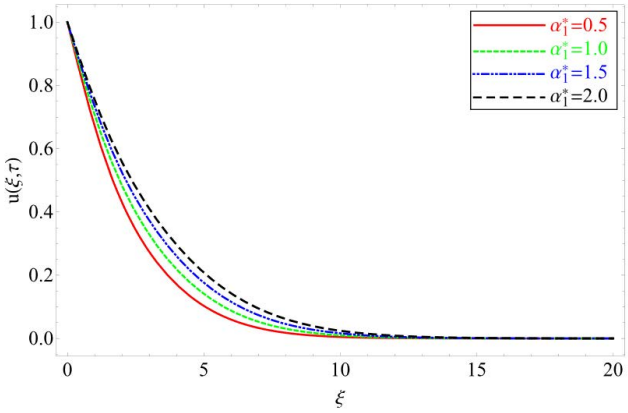

Figure 9. Variation in velocity profile against second-grade fluid parameter α_1^*

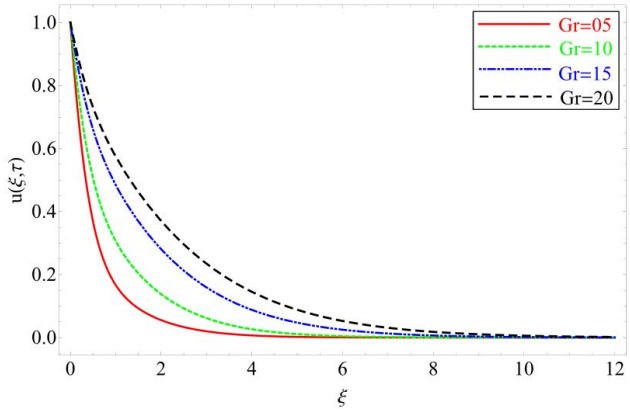

Figure 10. Variation in velocity profile against thermal Grashof number Gr

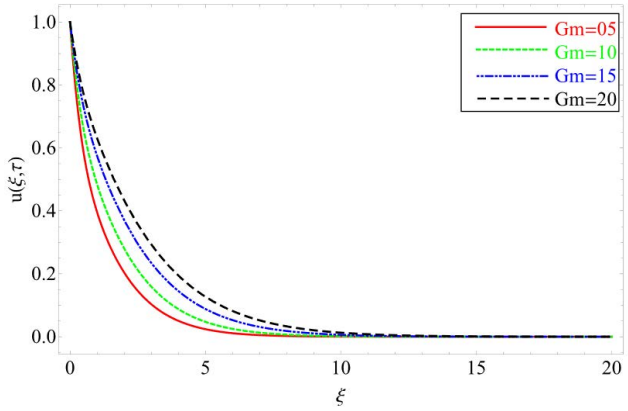

Figure 11. Variation in velocity profile against mass Grashof number Gm

Figure 12 examines the influence of variable order ρ on the velocity profile, keeping the other parameters constant. The identical pattern has been observed, as depicted in Figures 4 and 7. The findings demonstrate that the temperature distribution also exhibits an increase with higher values of the variable order ρ. The impact of the magnetic parameter is depicted in Figure 13, where the figure displays a diminishing variation in its profile with increasing magnitude of M. Fluid flow velocity profiles can be influenced by magnetic parameters M, which gauge the strength of the magnetic field in relation to fluid flow. As the magnetic parameter increases, fluid flow encounters stronger magnetic forces, augmenting the drag force on the fluid by opposing its motion. This increased drag force results in a decrease in fluid velocity. Furthermore, when a fluid flows through a magnetic field, it experiences a Lorentz force perpendicular to both the velocity and magnetic field directions, altering the fluid's momentum and

influencing its velocity and direction. Additionally, the magnetic field can induce alignment of the fluid in certain directions, altering fluid flow behavior and contributing to a reduction in the velocity profile. Magnetic parameters help a lot to control the fluid velocity in a medium and are tailored to achieve specific requirements.

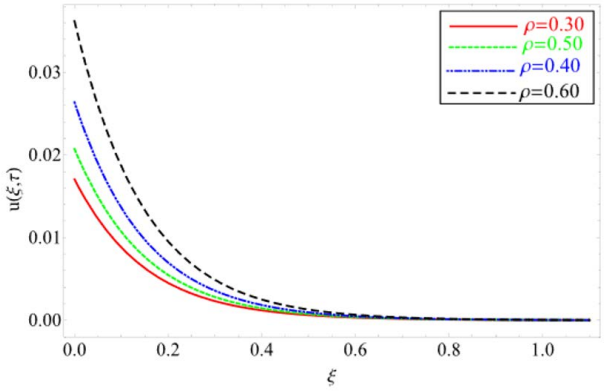

Figure 12. Variation in velocity profile against variable order ρ of Laplace transform

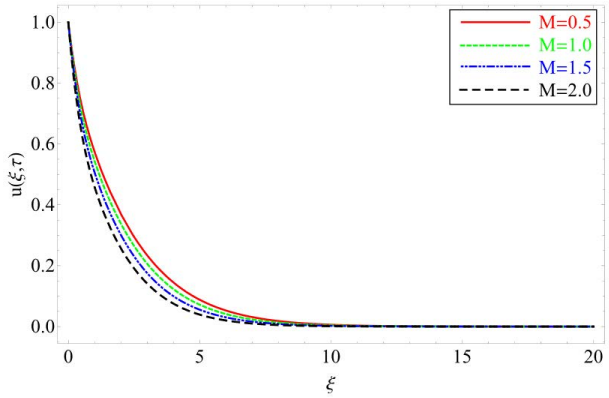

Figure 13. Variation in velocity profile against magnetic parameter M

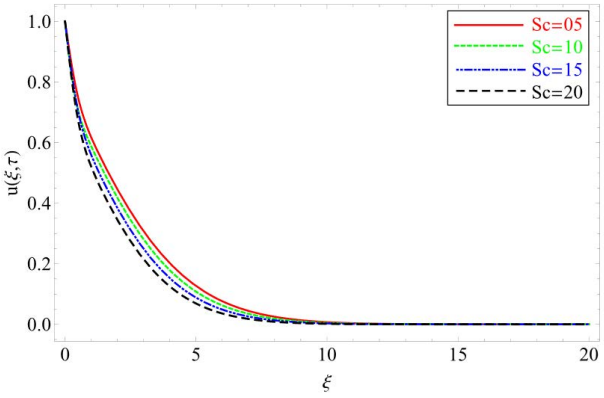

Figure 14. Variation in velocity profile against Schmidt number Sc

Figure 14 has been plotted to examine the fluid motion's reaction to the Schmidth number Sc. The relationship between momentum and mass transfer within a fluid is expressed by the Schmidt number, which acts as a dimensionless parameter. It quantifies how easily a substance can move through the fluid in comparison to its capacity to diffuse momentum, and is mathematically expressed as the ratio of kinematic viscosity to mass diffusivity. When the Schmidt number falls, it indicates a situation where the ratio of kinematic viscosity to mass diffusivity is relatively higher. This difference in mass transfer dynamics may noticeably affect the fluid's velocity profile. A lower Schmidt

number suggests a more effective mass transfer, demonstrating that a solute moves through a fluid more quickly than momentum is diffused. Essentially, this increased mass transfer can alter flow patterns by upsetting the typical velocity profile. The velocity profile was therefore elevated by a higher Schmidt number. Variations in fluid behavior in the reaction of volume fractions of Al_2O_3 have been plotted in Figure 15. In instances where volume fractions are low, the impact on viscosity tends to be negligible, thereby resulting in fluid behavior that closely resembles that of the base fluid. Nevertheless, with an increase in the volume fraction, the significance of particle-particle interactions becomes more pronounced. These interactions have the potential to induce alterations in the flow characteristics and viscosity. Hence, as the volume fraction of nanoparticles increases, there is a corresponding decrease in the velocity of the fluid.

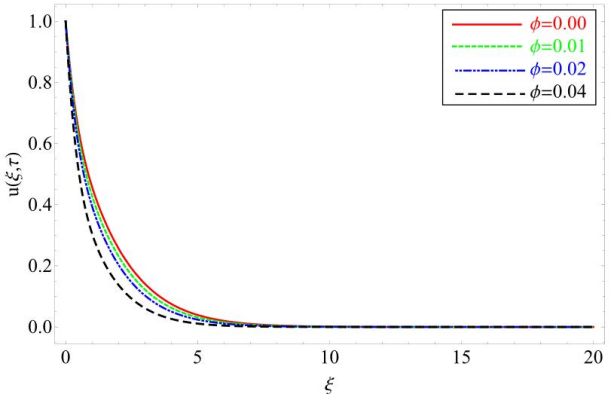

Figure 15. Variation in velocity profile against volume fraction ϕ of nanoparticle

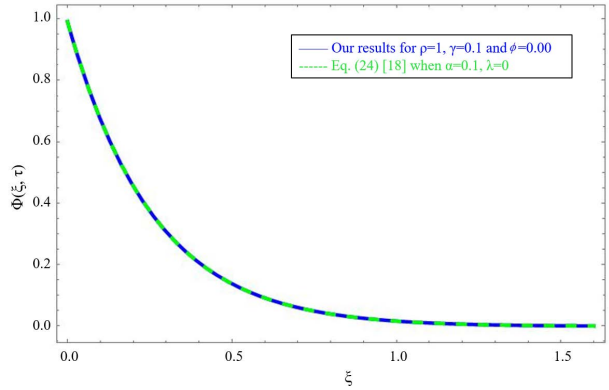

Figure 16. Concentration comparison with the study [23] (no presence of chemical reaction and nanoparticles)

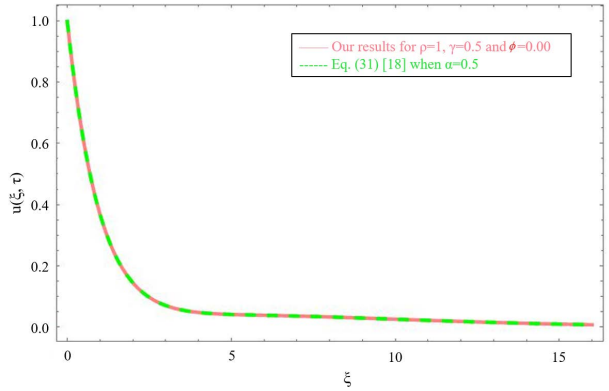

Figure 17. Velocity comparison with the study [23] (no presence of source of heat, chemical reaction and nanoparticles)

Figures 16 and 17 have been plotted for the sake of comparison and validation of the present work and obtained solutions. The authors have found that the present work has good agreement with already published work [18], which implies the correctness of the present calculi.

5 Concluding Remarks

The viscoelastic second grade nanofluid has been fractionalized on a vertical flat plate using the generalized Caputo fractional operator. Aluminium oxide Al_2O_3 nanomaterial was dispersed in mineral transformer oil to create a homogeneous mixture of nanofluid. The ρ-Laplace transform technique, which is more versatile than the standard Laplace transform technique, has been used to find solutions for generalized governing equations. The graphs of rooted parameters have been physically elaborated and represented by mathematical software for graphical analysis. The following list includes the main conclusions of the analysis:

• When comparing the classical model to the fractional parameter, it is observed that the latter yields multiple lines. The phenomenon serves as a demonstration of the memory effect exhibited by the fluid, a phenomenon that is not adequately explained by the classical model.

• By adjusting the value of ρ, γ and ϕ the obtained solution has been reduced to the already published work, which shows the correctness and validity of the mathematical model.

• By uniformly dispersing of Al_2O_3 nanoparticles in mineral transformer oil, the rate of heat transfer enhanced with 10.7407% as compared to regular MTO.

• Velocity field raised with the greater value of ρ, Gm, Gr and α_1^* while fall with ϕ, Sc, M and γ.

• Temperature field rises with the higher values of ρ and ϕ while fall with γ.

• Concentration field rises with the higher values of Sc and ϕ while fall with γ.

Data Availability

The data used to support the research findings are available from the corresponding author upon request.

Conflicts of Interest

The authors declare no conflict of interest.

References

[1] S. Murtaza, P. Kumam, Z. Ahmad, K. Sitthithakerngkiet, and T. Sutthibutpong, "Fractional model of brinkman-type nanofluid flow with fractional order Fourier's and Fick's laws," *Fractals*, vol. 31, no. 10, pp. 1–16, 2023. https://doi.org/10.1142/s0218348x23401990

[2] M. Bilal, A. Ali, S. R. Mahmoud, E. Tag-Eldin, and M. Balubaid, "Fractional analysis of unsteady radiative brinkman-type nanofluid flow comprised of CoFe2O3 nanoparticles across a vertical plate," *J. Therm. Anal. Calorim.*, vol. 148, no. 24, pp. 13 869–13 882, 2023. https://doi.org/10.1007/s10973-023-12705-0

[3] Kamran, S. U. Khan, S. Haque, and N. Mlaiki, "On the approximation of fractional-order differential equations using Laplace transform and weeks method," *Symmetry*, vol. 15, no. 6, p. 1214, 2023. https://doi.org/10.3390/sym15061214

[4] S. Ahmad, K. Shah, T. Abdeljawad, and B. Abdalla, "On the approximation of fractal-fractional differential equations using numerical inverse Laplace transform methods," *Comput. Model. Eng. Sci.*, vol. 135, no. 3, p. 2743, 2023. https://doi.org/10.32604/cmes.2023.023705

[5] H. M. Fahad, M. U. Rehman, and A. Fernandez, "On Laplace transforms with respect to functions and their applications to fractional differential equations," *Math. Methods Appl. Sci.*, vol. 46, no. 7, pp. 8304–8323, 2021. https://doi.org/10.1002/mma.7772

[6] S. Murtaza, F. Ali, Aamina, N. A. Sheikh, I. Khan, and K. S. Nisar, "Exact analysis of non-linear fractionalized Jeffrey fluid. A novel approach of Atangana–Baleanu fractional model," *Comput. Mater. Continua*, vol. 65, no. 3, pp. 2033–2047, 2020. https://doi.org/10.32604/cmc.2020.011817

[7] S. Murtaza, P. Kumam, Z. Ahmad, T. Seangwattana, and I. E. Ali, "Numerical analysis of newly developed fractal-fractional model of Casson fluid with exponential memory," *Fractals*, vol. 30, no. 5, pp. 1–10, 2022. https://doi.org/10.1142/s0218348x2240151x

[8] S. Murtaza, M. Iftekhar, F. Ali, Aamina, and I. Khan, "Exact analysis of non-linear electro-osmotic flow of generalized maxwell nanofluid: Applications in concrete based nanomaterials," *IEEE Access*, vol. 8, no. 1, pp. 96 738–96 747, 2020. https://doi.org/10.1109/access.2020.2988259

[9] S. Murtaza, F. Ali, N. A. Sheikh, I. Khan, and K. S. Nisar, "Analysis of silver nanoparticles in engine oil: Atangana-Baleanu fractional model," *Comput. Mater. Continua*, vol. 67, no. 3, pp. 2915–2932, 2021. https://doi.org/10.32604/cmc.2021.013757

[10] S. G. Samko, A. A. Kilbas, and O. I. Marichev, *Fractional Integrals and Derivatives: Theory and Applications*. Gordon and Breach Science Publishers, USA, 1993.

[11] A. Atangana and D. Baleanu, "New fractional derivative with non-local and non-singular kernel," *J. Therm. Sci.*, vol. 20, no. 2016, pp. 757–763, 2016. https://doi.org/10.48550/ARXIV.1602.03408

[12] M. Caputo and M. Fabrizio, "A new definition of fractional derivative without singular kernel," *Fract. Differ. Appl.*, vol. 1, pp. 73–85, 2015. https://doi.org/10.12785/pfda/010201

[13] F. Ali, S. Murtaza, N. A. Sheikh, and I. Khan, "Heat transfer analysis of generalized Jeffery nanofluid in a rotating frame: Atangana–Balaenu and Caputo–Fabrizio fractional models," *Chaos Solitons Fractals*, vol. 129, no. 29, pp. 1–15, 2019. https://doi.org/10.1016/j.chaos.2019.08.013

[14] J. Losada and J. J. Nieto, "Properties of a new fractional derivative without singular kernel," *Progr. Fract. Differ. Appl.*, vol. 1, no. 2015, pp. 87–92, 2015. https://doi.org/10.12785/pfda/010202

[15] M. Sinan, H. Ahmad, Z. Ahmad, J. Baili, S. Murtaza, M. Aiyashi, and T. Botmart, "Fractional mathematical modeling of malaria disease with treatment & insecticides," *Results Phys.*, vol. 34, no. 1, p. 105220, 2022. https://doi.org/10.1016/j.rinp.2022.105220

[16] T. Abdeljawad and D. Baleanu, "Integration by parts and its applications of a new nonlocal fractional derivative with Mittag-Leffler nonsingular kernel," *J. Nonlinear Sci. Appl.*, vol. 10, no. 3, pp. 1098–1107, 2017. https://doi.org/10.22436/jnsa.010.03.20

[17] S. Murtaza, P. Kumam, Z. Ahmad, K. Sitthithakerngkiet, and I. E. Ali, "Finite difference simulation of fractal-fractional model of electro-osmotic flow of Casson fluid in a micro channel," *IEEE Access*, vol. 10, no. 1, pp. 26 681–26 692, 2022. https://doi.org/10.1109/access.2022.3148970

[18] F. Jarad and T. Abdeljawad, "A modified Laplace transform for certain generalized fractional operators," *Results Nonlinear Anal.*, vol. 1, no. 2, pp. 88–98, 2018.

[19] M. Bilal, A. Saeed, M. M. Selim, T. Gul, I. Ali, and P. Kumam, "Comparative numerical analysis of Maxwell's time-dependent thermo-diffusive flow through a stretching cylinder," *Case Studi. Therm. Eng.*, vol. 27, no. 1, p. 101301, 2021. https://doi.org/10.1016/j.csite.2021.101301

[20] R. T. Alqahtani, S. Ahmad, and A. Akgül, "Dynamical analysis of bio-ethanol production model under generalized nonlocal operator in Caputo sense," *Mathematics*, vol. 9, no. 19, p. 2370, 2021. https://doi.org/10.3390/math9192370

[21] S. Ahmad, A. Ullah, A. Akgül, and M. De la Sen, "A study of fractional order Ambartsumian equation involving exponential decay kernel," *AIMS Math,*, vol. 6, no. 9, pp. 9981–9997, 2021. https://doi.org/10.3934/math.2021580

[22] N. Sene and A. N. Fall, "Homotopy perturbation ρ-Laplace transform method and its application to the fractional diffusion equation and the fractional diffusion-reaction equation," *Fractal Fract.*, vol. 3, no. 2, p. 14, 2019. https://doi.org/10.3390/fractalfract3020014

[23] M. Nazar, M .Ahmad, M. A. Imran, and N. A. Shah, "Double convection of heat and mass transfer flow of MHD generalized second grade fluid over an exponentially accelerated infinite vertical plate with heat absorption," *J. Math. Anal.*, vol. 8, no. 6, pp. 28–44, 2017.

[24] H. C. Brinkman, "The viscosity of concentrated suspensions and solutions," *J. Chem. Phys.*, vol. 20, no. 4, pp. 571–571, 1952. https://doi.org/10.1063/1.1700493

[25] S. M. Aminossadati and B. Ghasemi, "Natural convection cooling of a localised heat source at the bottom of a nanofluid-filled enclosure," *Eur. J. Mech. B*, vol. 28, no. 5, pp. 630–640, 2009. https://doi.org/10.1016/j.euromechflu.2009.05.006

[26] G. C. Bourantas and V. C. Loukopoulos, "Modeling the natural convective flow of micropolar nanofluids," *Int. J. Heat Mass Transfer*, vol. 68, no. 14, pp. 35–41, 2014. https://doi.org/10.1016/j.ijheatmasstransfer.2013.09.006

[27] J. C. Maxwell, *Electricity and Magnetism (Vol. 2)*. New York: Dover, 1954.

[28] SubsTech. Thermophysical properties of mineral transformer oil. http://www.substech.com/dokuwiki/doku.php?id=mineral_transformer_oil

[29] M. Dong, L. P. Shen, H. Wang, H. B. Wang, and J. Miao, "Investigation on the electrical conductivity of transformer oil-based AlN nanofluid," *J. Nanomater.*, 2013. https://doi.org/10.1155/2013/842963

[30] D. H. Fontes, G. Ribatski, and E. P. Bandarra Filho, "Experimental evaluation of thermal conductivity, viscosity and breakdown voltage AC of nanofluids of carbon nanotubes and diamond in transformer oil," *Diamond Relat. Mater.*, vol. 58, no. 1, pp. 115–121, 2015. https://doi.org/10.1016/j.diamond.2015.07.007

Nomenclature

u	Velocity component in x-axis
y	y-axis
t	Time
T	Temperature of the fluid
C	Concentration of the fluid
T_∞	Surrounding temperature
C_∞	Surrounding concentration
T_w	Temperature of the fluid on plate
C_w	Concentration of the fluid on plate
U_0	Characteristic velocity
$H(t)$	Heaviside step function
$\exp(t)$	Exponential function

Greek symbols

ρ	Density
μ	Dynamic viscosity
σ	Electrical conductivity
$\rho\beta_T$	Thermal expansion coefficient
$\rho\beta_C$	Volumetric expansion
ρC_p	Specific heat capacity
k	Thermal conductivity
D	Mass diffusion coefficient
ϕ	Volume fraction parameter
γ	Fractional parameter
α_1^*	Second grade fluid parameter
$\rho-$	Variable order of the Laplace transform

Subscripts

nf	Nanofluid
f	Base fluid
s	Nanoparticle